

Artificial GAN Fingerprints: Rooting Deepfake Attribution in Training Data

Ning Yu^{1,2*} Vladislav Skripniuk^{3*} Sahar Abdelnabi³ Mario Fritz³

¹University of Maryland, College Park, United States

²Max Planck Institute for Informatics, Saarbrücken, Germany

³CISPA Helmholtz Center for Information Security, Saarbrücken, Germany

{ningyu, vladislav}@mpi-inf.mpg.de

{sahar.abdelnabi, fritz}@cispa.saarland

Abstract

*Photorealistic image generation has reached a new level of quality due to the breakthroughs of generative adversarial networks (GANs). Yet, the dark side of such deepfakes, the malicious use of generated media, raises concerns about visual misinformation. While existing research work on deepfake detection demonstrates high accuracy, it is subject to advances in generation technologies and the adversarial iterations on detection countermeasure techniques. Thus, we seek a proactive and sustainable solution on deepfake detection, that is agnostic to the evolution of GANs, by introducing **artificial fingerprints** into the generated images.*

*Our approach first embeds fingerprints into the training data, we then show a surprising discovery on the **transferability** of such fingerprints from training data to GAN models, which in turn enables reliable detection and attribution of deepfakes. Our empirical study shows that our fingerprinting technique (1) holds for different state-of-the-art GAN configurations, (2) gets more effective along with the development of GAN techniques, (3) has a negligible side effect on the generation quality, and (4) stays robust against image-level and model-level perturbations. Our solution enables the responsible disclosure and regulation of such double-edged techniques and introduces a sustainable margin between real data and deepfakes, which makes this solution independent of the current arms race.*

1. Introduction

In the past years, photorealistic image generation has been rapidly evolving, benefiting from the invention of generative adversarial networks (GANs) [12] and its successive breakthroughs [31, 13, 28, 2, 20, 21, 22]. Given the level of realism and diversity that GANs can achieve today, detecting generated media, well known as *deepfakes*, attributing

their sources, and tracing their legal responsibilities become infeasible to human beings.

Moreover, the misuse of deepfakes has been permeating to each corner of social media, ranging from misinformation of political campaigns [19] to fake journalism [36, 32]. This motivates tremendous research efforts on deepfake detection [43] and source attribution [27, 42, 38]. These techniques aim to counter the widespread of malicious applications of deepfakes by automatically identifying and flagging generated visual contents and tracking their sources. Most of them rely on low-level visual patterns in GAN-generated images [27, 42, 38] or frequency mismatch [9, 45, 10]. However, these techniques are unlikely to sustainably and robustly stop deepfake misuse in the long run; as GANs evolve, they learn to better match the true distribution causing fewer artifacts [43]. For example, [8] proposes to conceal high-frequency cues of generated images, resulting in significant performance deterioration of state-of-the-art deepfake detectors. In addition, deepfake detectors are themselves vulnerable to adversarial evasion attacks [3, 43].

Motivated by this, we tackle deepfake detection and attribution through a different lens, and propose a sustainable solution for detection. In specific, we aim to introduce **artificial fingerprints** in the generated images that enable identification and tracing. Figure 1 depicts our pipeline; we first embed artificial fingerprints into the training data using a steganography model [1, 35]. The GAN model is then trained normally without modification. Thus, our solution is generalizable and agnostic to GAN configuration. We then show a surprising discovery on the **transferability** of such fingerprints from training data to the GAN model; the same fingerprint information that was encoded in the training data can be decoded from all generated images.

We achieve deepfake detection by classifying images with matched fingerprints in our database as fake and images with random detected fingerprints as real (because real images in fact do not contain artificial fingerprints). We also achieve deepfake attribution when we allocate different fin-

*Equal contribution.

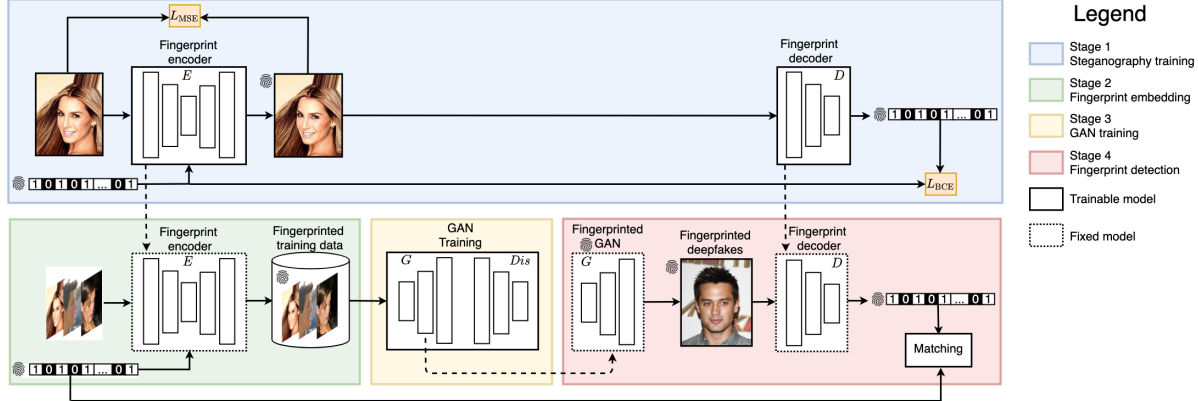


Figure 1: Our solution pipeline consists of four stages as captioned in the legend. We first train an image steganography encoder and decoder and then use the encoder to embed artificial fingerprints into the GAN training data. We then train a GAN model in the default way. Finally, we decode the fingerprints from the deepfakes; artificial fingerprints can be transferred from real data to the deepfakes.

gerprints for different GAN models. Our solution can thus prevent the misuse of a released trained GAN model by enabling publishers to proactively and responsibly introduce artificial fingerprints in their publicized models.

We summarize our contributions as follow:

1. Towards a sustainable solution that is independent of the current arms race, we propose the first *active* solution for deepfake detection and attribution by model fingerprinting.
2. This is the first study to demonstrate the *transferability* of artificial fingerprints from GAN training data to GAN models, which in turn justifies the feasibility for deepfake detection and attribution.
3. Our empirical study validates several beneficial properties of our solution. **Generality**: it holds for several state-of-the-art GAN configurations. **Synergy** with GANs: it gets more effective with the development of GAN techniques. **Fidelity**: it has a negligible side effect on generation quality. **Robustness**: it stays robust against image-level and model-level perturbations. **Secrecy**: the artificial fingerprints are not easy to detect by adversaries.

2. Related Work

Generative adversarial networks (GANs). GANs [12] was first proposed as a workaround to model the intractable real data distribution. The iterative improvements push the generation realism to brand-new levels [31, 13, 28, 2, 20, 21, 22]. Successes have also spread to many other vision tasks (e.g. texture synthesis [41], semantic image synthesis [29], super-resolution [23], image attribute editing [6], image to image translation [18, 47, 48], and inpainting [40]). In Section 5, we focus on unconditional GANs as

the subject of our study and work on the following three recent state-of-the-art GAN techniques: ProGAN [20], StyleGAN [21], and StyleGAN2 [22].

Deepfake detection and attribution. Images generated by GANs bear unique patterns. [27] shows that GANs leave unique noise residuals to generated samples, which facilitate deepfake detection. [42] moves one step further, using a neural network classifier to attribute different images to their sources. [38] also train a classifier and improve the generalization across different GAN techniques. [45, 9, 8] point out that the high-frequency pattern mismatch can serve as an effective cue for deepfake detection, so can the texture feature mismatch [26].

However, these cues are not sustainable because the advancement of deepfake detection is accompanied by further generation advancement in addition to detection countermeasure techniques. For example, spectral regularization [8] is proposed to narrow down the frequency mismatch and results in a significant detection deterioration. Also, state-of-the-art detectors (e.g. [38]) were found vulnerable to adversarial evasion attacks [3].

In contrast to the previous passive approaches, we propose a novel *active* solution for GAN fingerprinting and, thus, deepfake detection. We differentiate between the term *artificial fingerprints* which we use to refer to the information we deliberately and actively embed into the GAN model, and GAN fingerprints [42] which refer to the inherent cues and artifacts of different GAN models that were used in previous passive detection approaches.

Image steganography. Image steganography represents a technique to hide information into carrier images [11]. Previous steganography techniques [7, 4] rely on Fourier trans-

form or least significant bits modification [30, 16, 17]. Recent works substitute hand-crafted hiding procedures with neural network embedding [1, 14, 37, 44, 35]. In this work, we leverage recent deep learning-based steganography techniques [1, 35] to embed artificial fingerprints into training data. The stealthiness achieved by steganography allows preserving the original GAN quality, which is validated in Section 5.3. Our study is different from image steganography or digital watermarking techniques because our objective is to encode information to GAN model parameters such that all the generated images contain that information. This property is non-trivial and is justified in Section 5.2.

3. Problem Statement

Generation techniques can be used by adversaries or malicious parties in order to create visual misinformation and a possible flood of fake multimedia to achieve financial or political gains. Recently, there have been concerns about releasing generative models, e.g. OpenAI at first refused to release their GPT-2 language model, and they later employed a staged release to evaluate the potential risks [34].

Our fingerprinting solution introduces traceable artificial fingerprints in the generated images, which enables deepfake detection and attribution by decoding the fingerprints and matching them to the set of known fingerprints given to different models. This helps towards providing GAN publishers with a means for a proactive and responsible disclosure and publishing of their trained GAN models. This distinguishes our model fingerprinting solution from simply watermarking the generated images: we aim to defend against the malicious use of deepfakes generated by published GAN sources.

The artificial fingerprints’ encoder and decoder, and the unique identifier given for different GAN models, can be regulated by the cooperation among models’ publishers, or possibly by an independent regulatory authority. News or social media platforms could cooperate with models’ publishers to have a copy of the artificial fingerprint decoder and to maintain a database of fingerprints given to different models. The platform will then be able to detect and trace deepfakes generated by these models using the decoder.

4. Artificial Fingerprints for Deepfake Detection/Attribution

The goal of image attribution is to learn a mapping $D_0(\mathbf{x}) \mapsto y$ that traces the source $y \in \mathbb{Y} = \{\text{real}, \text{GAN}_1, \dots, \text{GAN}_N\}$ of an image \mathbf{x} . If the domain \mathbb{Y} is limited, predefined, and known to us, this is a closed-world scenario and the attribution can be simply formulated as a multi-label classification problem, each label corresponding to one source. In practice, \mathbb{Y} can be unlimited, predefined, continuously evolving, and agnostic to us. This open-

world scenario is intractable using discriminative learning. In order to generalize our solution to being agnostic to the selection of GANs, we formulate the attribution as a regression mapping $D(\mathbf{x}) \mapsto \mathbf{w}$, where $\mathbf{w} \in \{0, 1\}^n$ is the source identity space and n is the dimension. We propose a pipeline to root the attribution down to the GAN training dataset $\tilde{\mathbf{x}} \in \tilde{\mathbb{X}}$ and close the loop of the regression D . We describe the pipeline stages (depicted in Figure 1) below:

Steganography training. The source identity is represented by the artificial fingerprints \mathbf{w} . We use a steganography system [1, 35] to learn an encoder $E(\tilde{\mathbf{x}}, \mathbf{w}) \mapsto \tilde{\mathbf{x}}_{\mathbf{w}}$ that embeds an arbitrary fingerprint \mathbf{w} (randomly sampled during training) into an arbitrary image $\tilde{\mathbf{x}}$. In the meanwhile, we couple E with a decoder $D(\tilde{\mathbf{x}}_{\mathbf{w}}) \mapsto \mathbf{w}$ to detect the fingerprint information from the image. E and D are formulated as convolutional neural networks with the following training losses:

$$\min_{E, D} \mathbb{E}_{\tilde{\mathbf{x}} \sim \tilde{\mathbb{X}}, \mathbf{w} \sim \{0, 1\}^n} L_{\text{BCE}}(\tilde{\mathbf{x}}, \mathbf{w}; E, D) + \lambda L_{\text{MSE}}(\tilde{\mathbf{x}}, \mathbf{w}; E) \quad (1)$$

$$L_{\text{BCE}}(\tilde{\mathbf{x}}, \mathbf{w}; E, D) = \frac{1}{n} \sum_{k=1}^n (\mathbf{w}_k \log \hat{\mathbf{w}}_k + (1 - \mathbf{w}_k) \log (1 - \hat{\mathbf{w}}_k)) \quad (2)$$

$$L_{\text{MSE}}(\tilde{\mathbf{x}}, \mathbf{w}; E) = \|\mathbf{E}(\tilde{\mathbf{x}}, \mathbf{w}) - \tilde{\mathbf{x}}\|_2^2 \quad (3)$$

$$\hat{\mathbf{w}} = D(E(\tilde{\mathbf{x}}, \mathbf{w})) \quad (4)$$

where \mathbf{w}_k and $\hat{\mathbf{w}}_k$ are the k^{th} bit of the input fingerprint and detected fingerprint separately; and λ is a hyper-parameter to balance the two objective terms. The binary cross-entropy term L_{BCE} guides the decoder to decode whatever fingerprint embedded by the encoder. The mean squared error term L_{MSE} penalizes any deviation of the stego image $E(\tilde{\mathbf{x}}, \mathbf{w})$ from the original image $\tilde{\mathbf{x}}$. The architectures of E and D are depicted in the supplementary material.

Artificial fingerprint embedding. In this step, we use the already trained E and D networks. We allocate each GAN training dataset $\tilde{\mathbb{X}}$ a unique fingerprint \mathbf{w} . We apply the trained E to each training image $\tilde{\mathbf{x}}$ and collect a fingerprinted training dataset $\tilde{\mathbb{X}}_{\mathbf{w}} = \{E(\tilde{\mathbf{x}}, \mathbf{w}) | \tilde{\mathbf{x}} \in \tilde{\mathbb{X}}\}$.

GAN training. Our solution is agnostic to GAN techniques and therefore does not add any complexities to the GAN training. We simply replace $\tilde{\mathbb{X}}$ with $\tilde{\mathbb{X}}_{\mathbf{w}}$ to train the GAN model in the original manner.

Artificial fingerprint decoding. We hypothesize the *transferability* of our artificial fingerprints from training data to GAN models: a well-trained generator $G_{\mathbf{w}}(\mathbf{z}) \mapsto \mathbf{x}_{\mathbf{w}}$ contains, in all generated images, the same fingerprint information \mathbf{w} (as embedded in the training data $\tilde{\mathbf{x}}_{\mathbf{w}}$). Thus,

the artificial fingerprint can be recovered from a generated image \mathbf{x}_w using the decoder D : $D(\mathbf{x}_w) \equiv \mathbf{w}$. Based on this transferability, we can formulate deepfake attribution as fingerprint matching using our decoder D .

Artificial fingerprint matching. To support robustness to post-generation modifications that could be applied to the generated images, we relax the matching of the decoded artificial fingerprints to a soft matching. We perform a null hypothesis test given the number of matching bits k between the decoded fingerprint $\tilde{\mathbf{w}}$ and the fingerprint \mathbf{w} used in GAN training. The null hypothesis H_0 is getting this number of successes (i.e. matching bits) by chance. Under the null hypothesis, the probability of matching bits (random variable X) follows a binomial distribution; the number of trials n is the number of bits in the fingerprint sequence, k is the number of successes where each bit has a 0.5 probability of success. We can then measure the p -value of the hypothesis test by computing the probability of getting k or higher matching bits under the null hypothesis:

$$Pr(X > k | H_0) = \sum_{i=k}^n \binom{n}{i} 0.5^n \quad (5)$$

The fingerprint is verified, $\tilde{\mathbf{w}} \sim \mathbf{w}$, if the null hypothesis results in a very low probability (p -value). It means that it is not very likely to get this sequence of correct bits by chance. Usually, when the p -value is smaller than 0.05, we reject the null hypothesis and regard $1 - p$ as the verification confidence.

5. Experiments

We describe the experimental setup in Section 5.1. We first evaluate the required proprieties of our solution: the transferability of our artificial fingerprint, its generality, and synergy in Section 5.2. We demonstrate its fidelity in Section 5.3. In Section 5.4, we evaluate the robustness and working ranges of our approach. In Section 5.5, we evaluate the secrecy of the artificial fingerprints. The transferability in turn enables accurate deepfake detection and attribution, which is evaluated and compared in Section 5.6 and 5.7 respectively. In addition, we articulate our network designs and training details in the supplementary material.

5.1. Setup

Datasets. We conduct experiments on CelebA human face dataset [25] with image size $128 \times 128 \times 3$, and LSUN bedroom scene dataset [39] with image size $128 \times 128 \times 3$. We train/evaluate on 150k/50k CelebA, and 50k/50k LSUN.

GAN models. Our solution is agnostic to GAN configurations. Without losing representativeness, we focus on three

recent state-of-the-art GAN architectures: ProGAN [20], StyleGAN [21], and StyleGAN2 [22] config E. Each model is trained from scratch with the official implementations.

5.2. Transferability

The transferability means that the artificial fingerprints that are embedded in the GAN training data also appear consistently in the GAN-generated data. This is a non-trivial hypothesis in Section 4 and needs to be justified by the fingerprint detection accuracy.

Evaluation. Fingerprints are represented as binary vectors $\mathbf{w} \in \{0, 1\}^n$. We use bitwise accuracy to evaluate the detection accuracy. We set $n = 100$ as suggested in [35].

Baseline. For comparison, we implement a straightforward baseline method. Instead of embedding fingerprints into GAN training data, we enforce fingerprint generation jointly with GAN training. That is, we train on clean data, and enforce each generated image to not only look realistic and approximating the real training data but also contain a specific fingerprint. Mathematically,

$$\min_{G, D} \max_{Dis} \mathbb{E}_{\mathbf{z} \sim \mathcal{N}(\mathbf{0}, \mathbf{I}), \tilde{\mathbf{x}} \sim \tilde{\mathbb{X}}} L_{\text{adv}}(\mathbf{z}, \tilde{\mathbf{x}}; G, Dis) + \eta \mathbb{E}_{\mathbf{z} \sim \mathcal{N}(\mathbf{0}, \mathbf{I}), \mathbf{w} \sim \{0, 1\}^n} L_{\text{BCE}}(\mathbf{z}, \mathbf{w}; G, D) \quad (6)$$

where G and Dis are the original generator and discriminator in the GAN framework, L_{adv} is the original GAN objective, and L_{BCE} is adapted from Eq. 2 where we replace $\hat{\mathbf{w}} = D(E(\tilde{\mathbf{x}}, \mathbf{w}))$ with $\hat{\mathbf{w}} = D(G(\mathbf{z}))$. η is set to 1.0 as a hyper-parameter to balance the two objective terms.

Results. We report the fingerprint detection accuracy in Table 1. We observe:

1. The “Data” rows are the detection accuracy on real data for sanity checks: it reaches the 100% saturated accuracy, indicating the effectiveness of the steganography technique on its own.
2. Our artificial fingerprints can be almost perfectly and confidently detected from generated images over varying datasets and GAN configurations, with accuracy ≥ 0.98 and p -value $< 10^{-19}$ on CelebA and LSUN, except for ProGAN on LSUN which is a challenging case as ProGAN is known to be not good at generating LSUN (original FID only 29.16). Our hypothesis on the *transferability* from training data to GAN models (i.e. generated data) is justified. As a result, artificial fingerprints are qualified for deepfake detection in Section 5.6 where only generated images contain fingerprints, and qualified for deepfake attribution in Section 5.7 where different GANs are trained with different fingerprints.

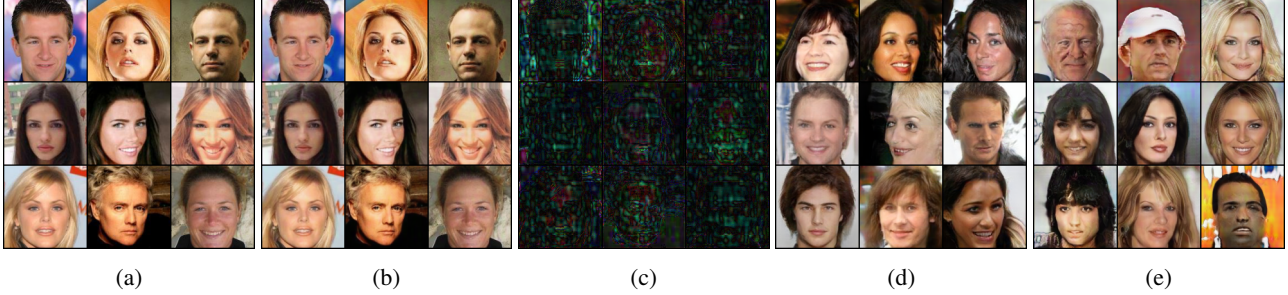


Figure 2: Samples for Table 1 on CelebA. (a) Original real training samples. (b) Fingerprinted real training samples. (c) The difference between (a) and (b). (d) Samples from the non-fingerprinted GAN. (e) Samples from the fingerprinted GAN. See more samples on LSUN in the supplementary material.

Table 1: Artificial fingerprint detection in bitwise accuracy (\uparrow indicates higher is better) and generation quality in FID (\downarrow indicates lower is better). The “Data” rows correspond to real testing images for a sanity check. The “Original FID” column corresponds to the generation quality of original (non-fingerprinted) GANs for references.

Dataset	Model	Bitwise accuracy \uparrow	p -value accepting H_0	Original FID \downarrow	Fingerprinted FID \downarrow
CelebA	Data	1.00	-	-	1.15
	ProGAN (bsl)	0.93	$< 10^{-19}$	14.09	60.28
	ProGAN	0.98	$< 10^{-26}$	14.09	14.38
	StyleGAN	0.99	$< 10^{-28}$	8.98	9.72
	StyleGAN2	0.99	$< 10^{-28}$	6.41	6.23
LSUN	Data	1.00	-	-	1.02
	ProGAN (bsl)	0.87	$< 10^{-14}$	29.16	183.63
	ProGAN	0.93	$< 10^{-19}$	29.16	32.58
	StyleGAN	0.98	$< 10^{-26}$	24.95	25.71
	StyleGAN2	0.99	$< 10^{-28}$	13.92	14.71

3. The *generality* of fingerprint transferability over varying GAN configurations justifies that our solution is agnostic to GAN techniques. Furthermore, along with the evolution of GANs (from ProGAN to StyleGAN and then to StyleGAN2), the fingerprint accuracy also improves, indicating the *synergy* between our solution and GANs: If a GAN technique can approximate real data distribution more accurately, it also transfers the artificial fingerprints more accurately. That makes our solution compatible with the advancements of GANs, unlike the detection approaches that rely on known GANs artifacts that could be enhanced.
4. The baseline method fails with fingerprint detection accuracy moderately worse than ours and FID far worse than ours and the original ones. This indicates GAN fingerprinting is a non-trivial task, and direct fingerprint reconstruction complicates the adversarial training. In contrast, our solution of leveraging image steganography and fingerprint transferability sidesteps this issue and leads to better performance.

5.3. Fidelity

The fidelity of generated images is as critical as the transferability (i.e. bitwise accuracy). The artificial fingerprints should have a negligible side effect on the original functionality of GANs. On one hand, it preserves the original generation quality. On the other hand, it avoids the adversary’s suspect of the presence of fingerprints. In principle, the steganography technique we used should enable this, and we validate it empirically.

Evaluation. We use Fréchet Inception Distance (FID) [15] to evaluate the generation quality; the lower, the more realistic. We measure FID between a set of 50k generated images and a set of 50k real non-fingerprinted images, in order to evaluate the quality of the former set. When calculating FID for different generations, the latter set is unchanged.

Results. We compare the generation quality of original and fingerprinted GANs in Table 1. We observe:

1. The “Data” rows are for sanity checks: embedding fingerprints on the real images does not substantially deteriorate image quality: $\text{FID} \leq 1.15$ is in an excellent realism range. That lays a valid foundation for high-quality GAN training.
2. The performance of the fingerprinted GANs tightly sticks to the performance limit of the non-fingerprinted baselines with the FID variance within a range of $\pm 8.2\%$ on CelebA and $\pm 11.7\%$ on LSUN. In practice, the fingerprints are imperceptibly hidden in the training images and can only be perceived with $10\times$ magnification. They are then imperceptibly transferred to the generated images. See Figure 2 for demonstrations. Thus, the fidelity of the fingerprinted GANs is justified and it qualifies our solution for deepfake detection and attribution in Section 5.6 and 5.7.

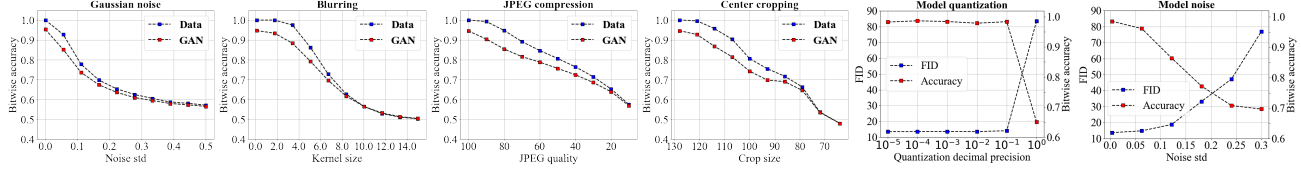


Figure 3: Zoom-in needed. Red plots show the artificial fingerprint detection in bitwise accuracy w.r.t. the amount of perturbations over ProGAN trained on CelebA. In the left four plots (robustness against image perturbations), blue dots represent detection accuracy on the fingerprinted real training images, which serve as the upper bound references for the red dots. See the supplementary material for additional results of ProGAN trained on LSUN. In the right two plots (robustness against model perturbations), blue dots represent the FID of generated images from the perturbed models.

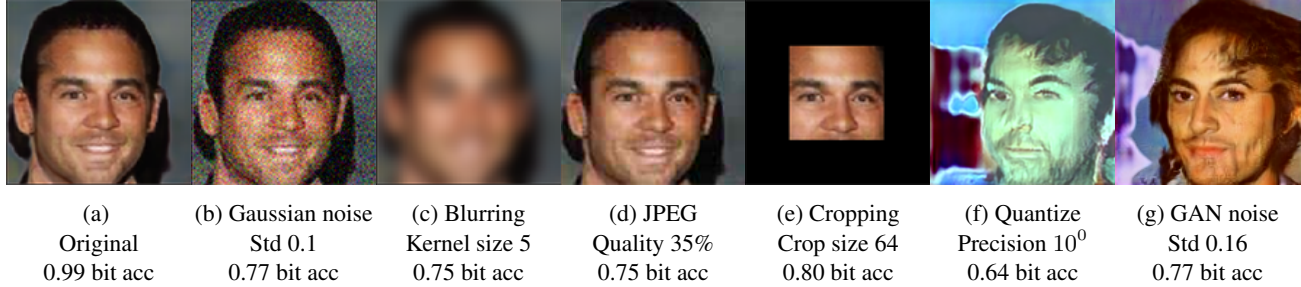


Figure 4: Perturbed image samples from the fingerprinted ProGAN and the corresponding fingerprint detection accuracy. The detection still performs robustly (bitwise accuracy ≥ 0.75) even when the image quality heavily deteriorates.

5.4. Robustness

Deepfake media and GAN models may undergo post-processing or perturbations during broadcasts. We validate the robustness of our fingerprint detection given a variety of image and model perturbations, and investigate the corresponding working ranges.

Perturbations. We evaluate the robustness against four types of image perturbation: additive Gaussian noise, blurring with Gaussian kernel, JPEG compression, center cropping. We also evaluate the robustness against two types of model perturbations: model weight quantization and adding Gaussian noise to model weights. For quantization, we compress each model weight given a decimal precision. We vary the amount of perturbations, apply each to the generated images or to the model directly, and detect the fingerprint using the pre-trained decoder.

Results. We evaluate the artificial fingerprint detection over 50k images from a fingerprinted ProGAN. We plot the bitwise accuracy w.r.t. the amount of perturbations in Figure 3 (see the supplementary material for additional results of ProGAN trained on LSUN). We observe:

1. For all the image perturbations, fingerprint detection accuracy drops monotonously as we increase the amount of perturbation, while for small perturbations

accuracy drops rather slowly. We consider accepting accuracy $\geq 75\%$ as a threshold ($p\text{-value} = 2.8 \times 10^{-7}$). This results in the working range w.r.t. each perturbation: Gaussian noise standard deviation $\sim [0.0, 0.05]$, Gaussian blur kernel size $\sim [0, 5]$, JPEG compression quality $\sim [50, 100]$, center cropping size $\sim [108, 128]$, quantization decimal precision $\leq 10^{-1}$, and model noise standard deviation $\sim [0.0, 0.18]$, which are reasonably wide ranges in practice.

2. For image perturbations (the left four subplots), outside the above working ranges, the reference upper bounds drop even faster and the margins to the testing curves shrink quickly, indicating that the detection deterioration is irrelevant to GAN training but rather relevant to the heavy quality deterioration of images.
3. For model perturbations (the right two subplots), outside the above working ranges, image quality deteriorates faster than fingerprint accuracy: even before the accuracy gets lower than 75%, FID has already increased by $> 500\%$.
4. As a result of (2) and (3), before fingerprint detection is close to random guess ($\sim 50\%$ accuracy), image quality has been heavily deteriorated by strong perturbations (Figure 4), which demonstrates that our fingerprints are more robust than image functionality itself in the case of these studied perturbations.

Discussion on attacks. Other attack scenarios that require training counter models might be conceivable. An example of such attacks is training a model to remove the fingerprints from generated images (e.g. a denoising autoencoder). However, this would require the attacker to have paired training data of images before and after the fingerprint embedding. In our scenario, we assume that the fingerprint encoder is not released by the publishers which hinders this training data collection requirement. Additionally, such attacks would require an adversary with more technical knowledge and powerful computational resources.

5.5. Secrecy

The presence of a fingerprint embedded in a GAN model should not be easily detected by a third party, otherwise, it would be potentially manipulated. This property is more demanding than fidelity because high fidelity just avoids intuitive detection while high secrecy requires technical counter-detection against steganalysis.

Attack. In order to design a quantitative evaluation of the secrecy, we formulate it as a binary classification problem: the presence of a fingerprint in an image. We follow the attack protocol in [46] to perform the Artificial Training Sets (ATS) attack [24]. We aim to classify between fingerprinted and non-fingerprinted test images (i.e. fingerprinted 0 or 1 time), but we have no supervision. The intuition is to expand the test set and establish an artificial setting with known labels which enables supervised training. The original test class space is now a subspace of the artificial training class space and is separable by the training task.

The attack is as follows: We independently trained another steganography encoder. We consider the original test images as negative training samples. Then, we apply the encoder twice to the test set to obtain extra images fingerprinted 2 times (corresponding to originally non-fingerprinted images) or 3 times (corresponding to originally fingerprinted images), which are regarded as positive training samples. Then we train an SVM classifier [5] using such positive and negative samples, in order to separate between images fingerprinted 0-1 time (original set), and the ones fingerprinted 2-3 times (artificial training set).

During testing, we first apply the encoder once to the test images so that the originally non-fingerprinted images are now fingerprinted 1 time (belonging to 0-1 class), and the originally fingerprinted images are now fingerprinted 2 times (belonging to 2-3 class). Then we can use the classifier to separate them and propagate the predictions back to the original images. We evaluate the attack on a set of 250 fingerprinted deepfake images and 250 non-fingerprinted deepfake images.

Results. The binary classification accuracy on the existence of fingerprint is **0.502** according to the ATS attack, which is close to random guess ($\sim 50\%$ accuracy). We reason that the third-party steganography encoder trained from different initialization uses different patterns to hide the fingerprint, and therefore does not couple well with the victim encoder. This also supports our previous discussion of the importance of keeping the encoder private to support both the secrecy and the robustness of the artificial fingerprints.

5.6. Deepfake Detection

In the previous sections, we demonstrated that our GAN fingerprinting solution is effective in transferring the fingerprints and keeping the generation quality while being robust against a range of attacks and maintaining secrecy against adversaries. We now discuss how to use this solution for deepfake detection and attribution.

Unlike existing methods that detect intrinsic differences between the real and deepfake classes [42, 45, 8], we propose an active solution by embedding artificial fingerprints into GAN models and consequently the generated images. Then we convert the problem to verifying if one decoded fingerprint is in our fingerprint regulation database or not. Even with a non-perfect detection accuracy, we still can use our solution based on the null hypothesis test. This is feasible based on two assumptions: (1) The decoded fingerprint of a real image is random; and (2) the fingerprint capacity is large enough such that the random fingerprint from a real image is unlikely to collide with a regulated fingerprint in the database. The second condition is trivial to satisfy considering we sample fingerprints $\mathbf{w} \in \{0, 1\}^n$ and $n = 100$. 2^{100} is a large enough capacity. Then we validate the first assumption by the deepfake detection experiments below.

Baseline. Without losing representativeness, we compare to a recent CNN-based deepfake detector [42] as a baseline method. It is trained on 50k real images and 50k generated images equally from four fingerprinted GANs. From the classifier’s perspective, we consider two scenarios, a *detection closed world* and a *detection open world* scenarios, depending on whether or not the set of GAN models used for the classifier training covers that used for testing. The open-world scenario challenges the classifier’s generalization. Our method is agnostic to the specific GAN model used and, therefore, the detection accuracy should be similar across all of these models, since the fingerprints’ encoder and decoder are pre-trained to embed and decode any arbitrary bit sequence $\mathbf{w} \in \{0, 1\}^n$. Thus, our solution does not have this open-world limitations. We assume that the pre-trained fingerprints’ encoder and decoder are fixed.

Results. We report deepfake detection accuracy in Table 2. We observe:

Table 2: Closed/open-world deepfake detection accuracy and attribution accuracy (\uparrow indicates higher is better).

Dataset	Model	Method	Deepfake detection		Deepfake attribution	
			Closed world	Open world	Closed world	Open world
CelebA	StyleGAN	[42]	0.997	0.508	0.998	0.235
		Ours	1.000	1.000	1.000	1.000
LSUN	StyleGAN2	[42]	0.994	0.497	0.999	0.168
		Ours	1.000	1.000	1.000	1.000
CelebA	StyleGAN2	[42]	0.995	0.500	1.000	0.267
		Ours	1.000	1.000	1.000	1.000
ProGAN	StyleGAN	[42]	1.000	0.493	0.986	0.597
		Ours	1.000	1.000	1.000	1.000
LSUN	StyleGAN	[42]	0.994	0.499	0.995	0.366
		Ours	1.000	1.000	1.000	1.000
LSUN	StyleGAN2	[42]	0.988	0.491	1.000	0.267
		Ours	1.000	1.000	1.000	1.000

1. Deepfake detection based on our fingerprints performs equally perfectly ($\sim 100\%$ accuracy) to that based on the CNN classifier in the closed world.
2. More advantageously, our solution performs equally well in the open-world scenario of the CNN classifier whose accuracy deteriorates to random guess ($\sim 50\%$ accuracy). This is because the CNN classifier is troubled by the domain gap between training and testing GAN models. In contrast, our solution enjoys the advantage of being agnostic to GAN models. It depends only on the presence of fingerprints rather than the discriminative information that overfit the closed world.
3. As a conclusion, this suggests the need for administrative coordination and cooperation of models’ publishers to responsibly and proactively fingerprint their publicized models or deepfake media.

Discussion on detection. While other more recent work demonstrated higher generalization to unseen GAN models [38] (i.e. detection in the open-world scenario), this success is still subject to future advances and evolution of GAN techniques, which were rapidly progressing over the last few years. In addition, the classifier in [38] was successfully evaded in [3] by extremely small perturbations. Therefore, our work offers higher sustainability in the long run by explicitly enforcing a margin between real and generated images.

5.7. Deepfake Attribution

The goal of the attribution is to trace the GAN source that generated a deepfake media. It plays an important role in tracing the responsible deepfake publisher. Our artificial fingerprint solution can be easily extended for attribution.

Attribution closed-world scenario. Here, the model space is finite and known in advance. Without losing generalization, we train four GAN models using four different fingerprints. The task is to attribute a mixture of 50k images evenly generated by these models. We apply our decoder to decode the fingerprint from an image, and assign that image to the GAN with the closest GAN fingerprint.

Attribution open-world scenario. Here, we should be able to identify if an image is generated from an unknown source. For the classifier, this means to identify that this is an unknown GAN. For our method, this means to identify that this specific fingerprint is not in the database of known fingerprints. We introduce another four GANs trained on unknown fingerprints and require to attribute another 12.5k images evenly generated by these four GANs, meaning to label them as not belonging to any of the four known GANs. Our fingerprint solution classifies an image as unknown if the number of matching bits between the detected fingerprint and the closest known fingerprint is less than 75%.

Baseline. [42] use a CNN classifier to solve deepfake attribution as a multi-class classification problem, which is limited to the closed world. We followed their protocol in the closed world scenario: training over 50k images generated evenly by each of the four GANs. We also extend their method to the open-world via training four one-vs-all-the-others binary classifiers. During testing, all four classifiers are applied to an image. We assign the image to the class with the highest confidence if not all the classifiers reject that image. Otherwise, it is assigned to the unknown label.

Results. We report deepfake attribution accuracy in Table 2. We obtain the same discoveries and conclusions as those of deepfake detection in Section 5.6. The open-world attribution deteriorates for the CNN classifier while our fingerprinting solution maintains a high accuracy.

6. Conclusion

Detecting deepfakes is a complex problem due to the rapid development of GANs and the possible adversarial countermeasure techniques. Towards a more sustainable solution, we investigate a fundamental active solution on the detection side that is agnostic to the evolution of GANs. We present the first study to embed artificial fingerprints into GAN models. We root deepfake detection/attribution into GAN training data, and demonstrate the transferability of artificial fingerprints from training data to GAN models. Our empirical study shows several beneficial properties of fingerprints, including generality, synergy with GAN development, fidelity, robustness, and secrecy. Based on this, we

demonstrate our advantageous detection and attribution performance on multiple datasets and GAN subjects. As there have been recent concerns about the release of generative technologies, our solution enables GAN publishers to responsibly and proactively fingerprint their publicized models or generated media, and opens up possibilities of regulation on the GAN disclosure process by allocating each publisher a unique fingerprint.

Acknowledgement

Ning Yu is partially supported by Twitch Fellowship. Vladislav Skripniuk is partially supported by IMPRS scholarship from Max Planck Institute. We acknowledge Matthew Tancik for his StegaStamp GitHub repository¹. We acknowledge Tero Karras for his ProGAN GitHub repository² and StyleGAN2 GitHub repository³. We also thank Apratim Bhattacharyya for constructive discussion and advice.

References

- [1] Shumeet Baluja. Hiding images in plain sight: Deep steganography. In *NeurIPS*, 2017. [1](#), [3](#)
- [2] Andrew Brock, Jeff Donahue, and Karen Simonyan. Large scale gan training for high fidelity natural image synthesis. In *ICLR*, 2018. [1](#), [2](#)
- [3] Nicholas Carlini and Hany Farid. Evading deepfake-image detectors with white-and black-box attacks. In *CVPR Workshops*, 2020. [1](#), [2](#), [8](#)
- [4] Francois Cayre, Caroline Fontaine, and Teddy Furon. Watermarking security: theory and practice. In *TSP*, 2005. [2](#)
- [5] Chih-Chung Chang and Chih-Jen Lin. Libsvm: A library for support vector machines. In *TIST*, 2011. [7](#)
- [6] Yunjey Choi, Minje Choi, Munyoung Kim, Jung-Woo Ha, Sunghun Kim, and Jaegul Choo. Stargan: Unified generative adversarial networks for multi-domain image-to-image translation. In *CVPR*, 2018. [2](#)
- [7] Ingemar Cox, Matthew Miller, Jeffrey Bloom, and Chris Honsinger. *Digital watermarking*. Springer, 2002. [2](#)
- [8] Ricard Durall, Margret Keuper, and Janis Keuper. Watch your up-convolution: Cnn based generative deep neural networks are failing to reproduce spectral distributions. In *CVPR*, 2020. [1](#), [2](#), [7](#)
- [9] Ricard Durall, Margret Keuper, Franz-Josef Pfreundt, and Janis Keuper. Unmasking deepfakes with simple features. *arXiv*, 2019. [1](#), [2](#)
- [10] Joel Frank, Thorsten Eisenhofer, Lea Schönherr, Asja Fischer, Dorothea Kolossa, and Thorsten Holz. Leveraging frequency analysis for deep fake image recognition. In *ICML*, 2020. [1](#)
- [11] Jessica Fridrich. *Steganography in digital media: principles, algorithms, and applications*. Cambridge University Press, 2009. [2](#)
- [12] Ian Goodfellow, Jean Pouget-Abadie, Mehdi Mirza, Bing Xu, David Warde-Farley, Sherjil Ozair, Aaron Courville, and Yoshua Bengio. Generative adversarial nets. In *NeurIPS*, 2014. [1](#), [2](#)
- [13] Ishaan Gulrajani, Faruk Ahmed, Martin Arjovsky, Vincent Dumoulin, and Aaron C Courville. Improved training of wasserstein gans. In *NeurIPS*, 2017. [1](#), [2](#)
- [14] Jamie Hayes and George Danezis. Generating steganographic images via adversarial training. In *NeurIPS*, 2017. [3](#)
- [15] Martin Heusel, Hubert Ramsauer, Thomas Unterthiner, Bernhard Nessler, and Sepp Hochreiter. Gans trained by a two time-scale update rule converge to a local nash equilibrium. In *NeurIPS*, 2017. [5](#)
- [16] Vojtěch Holub and Jessica Fridrich. Designing steganographic distortion using directional filters. In *WIFS*, 2012. [3](#)
- [17] Vojtěch Holub, Jessica Fridrich, and Tomáš Denemark. Universal distortion function for steganography in an arbitrary domain. In *EURASIP JIS*, 2014. [3](#)
- [18] Phillip Isola, Jun-Yan Zhu, Tinghui Zhou, and Alexei A Efros. Image-to-image translation with conditional adversarial networks. In *CVPR*, 2017. [2](#)
- [19] Charlotte Jee. An indian politician is using deepfake technology to win new voters. 2020. [1](#)
- [20] Tero Karras, Timo Aila, Samuli Laine, and Jaakko Lehtinen. Progressive growing of gans for improved quality, stability, and variation. In *ICLR*, 2018. [1](#), [2](#), [4](#), [11](#)
- [21] Tero Karras, Samuli Laine, and Timo Aila. A style-based generator architecture for generative adversarial networks. In *CVPR*, 2019. [1](#), [2](#), [4](#), [11](#)
- [22] Tero Karras, Samuli Laine, Miika Aittala, Janne Hellsten, Jaakko Lehtinen, and Timo Aila. Analyzing and improving the image quality of stylegan. In *CVPR*, 2020. [1](#), [2](#), [4](#), [11](#)
- [23] Christian Ledig, Lucas Theis, Ferenc Huszár, Jose Caballero, Andrew Cunningham, Alejandro Acosta, Andrew Aitken, Alykhan Tejani, Johannes Totz, Zehan Wang, et al. Photo-realistic single image super-resolution using a generative adversarial network. In *CVPR*, 2017. [2](#)
- [24] Daniel Lerch-Hostalot and David Megías. Unsupervised steganalysis based on artificial training sets. In *EAAI*, 2016. [7](#)
- [25] Ziwei Liu, Ping Luo, Xiaogang Wang, and Xiaoou Tang. Deep learning face attributes in the wild. In *ICCV*, 2015. [4](#)
- [26] Zhenghe Liu, Xiaojuan Qi, Jiaya Jia, and Philip Torr. Global texture enhancement for fake face detection in the wild. In *CoRR*, 2020. [2](#)
- [27] Francesco Marra, Diego Gragnaniello, Luisa Verdoliva, and Giovanni Poggi. Do gans leave artificial fingerprints? In *MIPR*, 2019. [1](#), [2](#)
- [28] Takeru Miyato, Toshiki Kataoka, Masanori Koyama, and Yuichi Yoshida. Spectral normalization for generative adversarial networks. In *ICLR*, 2018. [1](#), [2](#)

¹<https://github.com/tancik/StegaStamp>

²https://github.com/tkarras/progressive_growing_of_gans

³<https://github.com/NVlabs/stylegan2>

[29] Taesung Park, Ming-Yu Liu, Ting-Chun Wang, and Jun-Yan Zhu. Semantic image synthesis with spatially-adaptive normalization. In *CVPR*, 2019. 2

[30] Tomáš Pevný, Tomáš Filler, and Patrick Bas. Using high-dimensional image models to perform highly undetectable steganography. In *IWIH*, 2010. 3

[31] Alec Radford, Luke Metz, and Soumith Chintala. Unsupervised representation learning with deep convolutional generative adversarial networks. In *ICLR*, 2016. 1, 2

[32] Dan Robitzski. Someone used deepfake tech to invent a fake journalist. 2020. 1

[33] Olaf Ronneberger, Philipp Fischer, and Thomas Brox. U-net: Convolutional networks for biomedical image segmentation. In *MICCAI*, 2015. 11

[34] Irene Solaiman, Miles Brundage, Jack Clark, Amanda Askell, Ariel Herbert-Voss, Jeff Wu, Alec Radford, Gretchen Krueger, Jong Wook Kim, Sarah Kreps, et al. Release strategies and the social impacts of language models. *arXiv*, 2019. 3

[35] Matthew Tancik, Ben Mildenhall, and Ren Ng. Stegastamp: Invisible hyperlinks in physical photographs. In *CVPR*, 2020. 1, 3, 4, 11

[36] James Vincent. An online propaganda campaign used ai-generated headshots to create fake journalists. 2020. 1

[37] Vedran Vukotić, Vivien Chappelier, and Teddy Furon. Are deep neural networks good for blind image watermarking? In *WIFS*, 2018. 3

[38] Sheng-Yu Wang, Oliver Wang, Richard Zhang, Andrew Owens, and Alexei A Efros. Cnn-generated images are surprisingly easy to spot... for now. In *CVPR*, 2020. 1, 2, 8

[39] Fisher Yu, Ari Seff, Yinda Zhang, Shuran Song, Thomas Funkhouser, and Jianxiong Xiao. Lsun: Construction of a large-scale image dataset using deep learning with humans in the loop. *arXiv*, 2015. 4

[40] Jiahui Yu, Zhe Lin, Jimei Yang, Xiaohui Shen, Xin Lu, and Thomas S Huang. Generative image inpainting with contextual attention. In *CVPR*, 2018. 2

[41] Ning Yu, Connelly Barnes, Eli Shechtman, Sohrab Amirghodsí, and Michal Lukac. Texture mixer: A network for controllable synthesis and interpolation of texture. In *CVPR*, 2019. 2

[42] Ning Yu, Larry S Davis, and Mario Fritz. Attributing fake images to gans: Learning and analyzing gan fingerprints. In *ICCV*, 2019. 1, 2, 7, 8

[43] Baiwu Zhang, Jin Peng Zhou, Ilia Shumailov, and Nicolas Papernot. Not my deepfake: Towards plausible deniability for machine-generated media. *arXiv*, 2020. 1

[44] Ru Zhang, Shiqi Dong, and Jianyi Liu. Invisible steganography via generative adversarial networks. In *Multimedia Tools and Applications*, 2019. 3

[45] Xu Zhang, Svebor Karaman, and Shih-Fu Chang. Detecting and simulating artifacts in gan fake images. In *WIFS*, 2019. 1, 2, 7

[46] Jiren Zhu, Russell Kaplan, Justin Johnson, and Li Fei-Fei. Hidden: Hiding data with deep networks. In *ECCV*, 2018. 7

[47] Jun-Yan Zhu, Taesung Park, Phillip Isola, and Alexei A Efros. Unpaired image-to-image translation using cycle-consistent adversarial networks. In *ICCV*, 2017. 2

[48] Jun-Yan Zhu, Richard Zhang, Deepak Pathak, Trevor Darrell, Alexei A Efros, Oliver Wang, and Eli Shechtman. Toward multimodal image-to-image translation. In *NeurIPS*, 2017. 2

7. Supplementary material

A. Implementation Details

Steganography encoder. The encoder is trained to embed a fingerprint into an image while minimizing the pixel difference between the input and stego images. We follow the technical details in [35]. The binary fingerprint vector is first passed through a fully-connected layer and then reshaped as a tensor with one channel dimension and with the same spatial dimension of the cover image. We then concatenate this fingerprint tensor and the image along the channel dimension as the input to a U-Net architecture [33]. The output of the encoder, the stego image, has the same size as that of the input image. Note that passing the fingerprint through a fully-connected layer allows for every bit of the binary sequence to be encoded over the entire spatial dimensions of the input image and flexible to the image size. In our experiments, the image size is set to $128 \times 128 \times 3$ without losing representativeness. The fingerprint length is set to 100 as suggested in [35]. The length of 100 bits leads to a large enough space for fingerprint allocation while not having a side effect on the fidelity performance. We visualize the encoder architecture in Figure 5.

Steganography decoder. The decoder is trained to detect the hidden fingerprint from the stego image. We follow the technical details in [35]. It consists of a series of convolutional layers with kernel size 3x3 and strides ≥ 1 , dense layers, and a sigmoid output activation to produce a final output with the same length as the binary fingerprint vector. We visualize the encoder architecture in Figure 6.

Steganography training. The encoder and decoder are jointly trained end-to-end w.r.t. the objective in Eq. 1 in the main paper and with randomly sampled fingerprints. The encoder is trained to balance fingerprint detection and image reconstruction. At the beginning of training, we set $\lambda = 0$ to focus on fingerprint detection, otherwise, fingerprints cannot be accurately embedded into images. After the fingerprint detection accuracy achieves 95% (that takes 3-5 epochs), we increase λ linearly up to 10 within 3k iterations to shift our focus more on image reconstruction. We train the encoder and decoder for 30 epochs in total. Given the batch size of 64, it takes 3 hours using 1 NVIDIA Tesla V100 GPU with 16GB memory.

GAN training. Our fingerprinting method is favorably agnostic to GAN techniques because we only process the training data. Therefore, for GAN training, we directly refer to the corresponding GitHub repositories of GANs with-

out any change: ProGAN [20]⁴, StyleGAN [21] and StyleGAN2 [22] (config E)⁵.

B. Samples on LSUN

See Figure 7 for fingerprinted samples on LSUN. We obtain the same conclusion as in Section 5.3 in the main paper: The fingerprints are imperceptibly hidden in the training images and can only be perceived with $10\times$ magnification. They are then imperceptibly transferred to the generated images.

C. Robustness of ProGAN on LSUN

For the robustness of ProGAN on LSUN, we plot the bitwise accuracy w.r.t. the amount of perturbations in Figure 8. We obtain the same conclusions as those in Section 5.4 in the main paper. In specific, the working range w.r.t. each perturbation: Gaussian noise standard deviation $\sim [0.0, 0.1]$, Gaussian blur kernel size $\sim [0, 7]$, JPEG compression quality $\sim [30, 100]$, and center cropping size $\sim [108, 128]$, which are reasonably wide ranges in practice.

⁴https://github.com/tkarras/progressive_growing_of_gans

⁵<https://github.com/NVlabs/stylegan2>

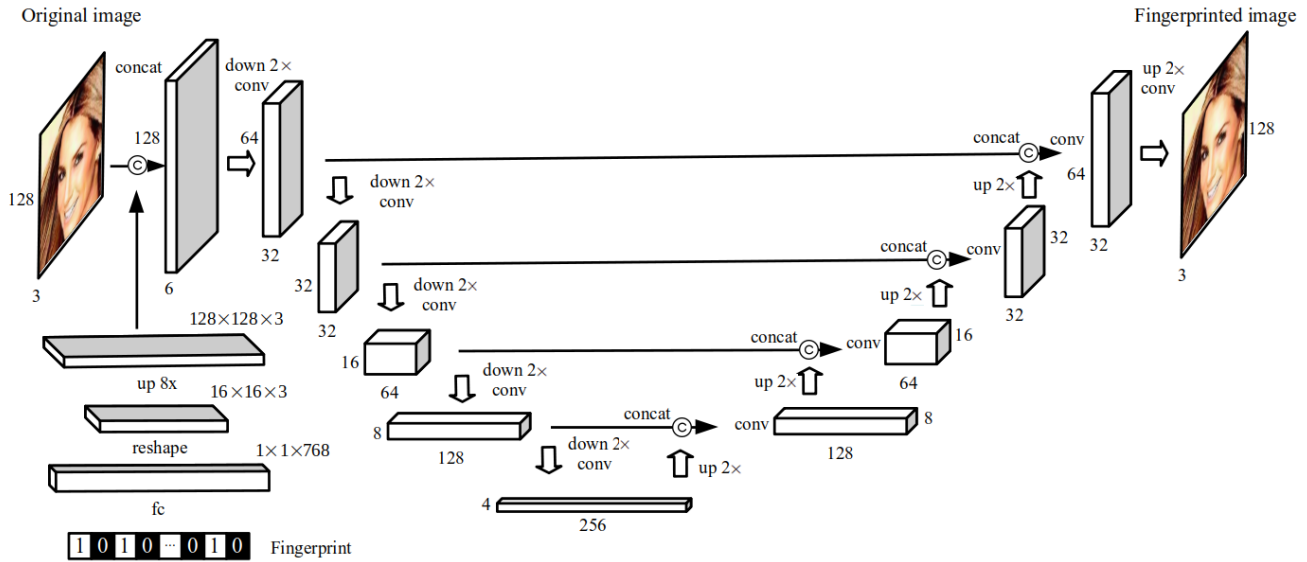


Figure 5: Steganography encoder architecture.

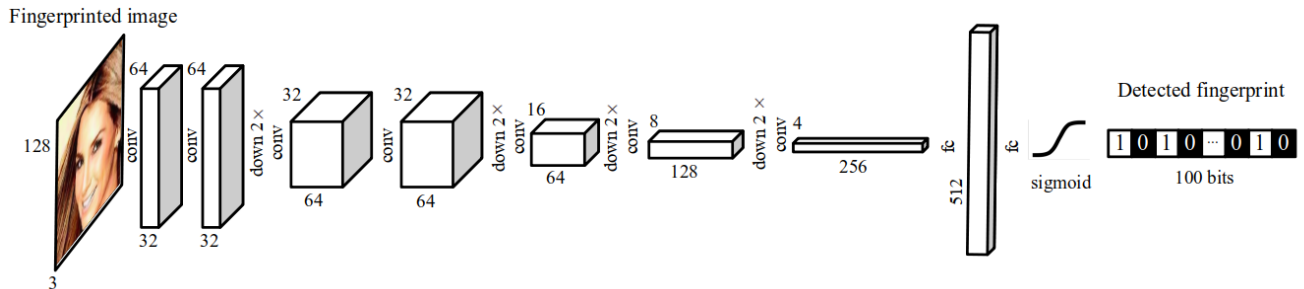


Figure 6: Steganography decoder architecture.

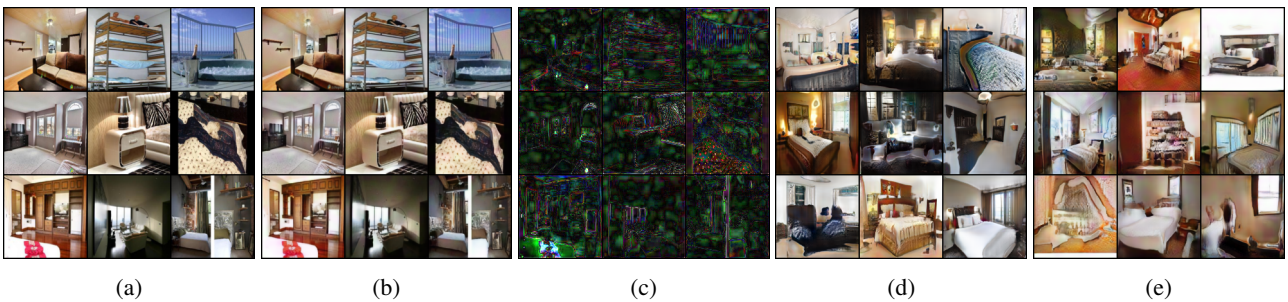


Figure 7: Samples on LSUN for Table 1 in the main paper, supplementary to Figure 2 in the main paper. (a) Original real training samples. (b) Fingerprinted real training samples. (c) The difference between (a) and (b). (d) Samples from the non-fingerprinted GAN. (e) Samples from the fingerprinted GAN.

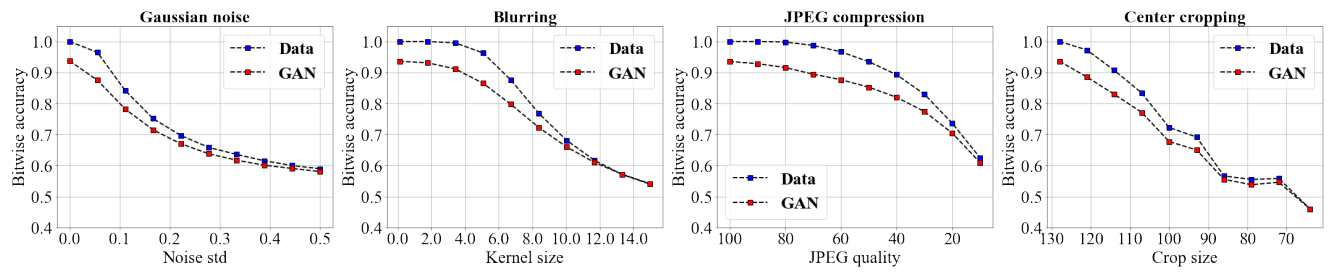


Figure 8: Zoom-in needed. Red plots show the artificial fingerprint detection in bitwize accuracy w.r.t. the amount of perturbations over ProGAN trained on LSUN. Blue dots represent detection accuracy on the fingerprinted real training images, which serve as the upper bound references for the red dots. This is supplementary to Figure 3 in the main paper.